Heat Transfer—Asian Research, **41** (6), 2012

Effect of Viscosity Variation on Natural Convection Flow of Water–Alumina Nanofluid in an Annulus with Internal Heat Generation

Rehena Nasrin,[1] M.A. Alim,[1] and Ali J. Chamkha[2]
[1]Department of Mathematics, Bangladesh University of Engineering & Technology, Dhaka, Bangladesh
[2]Manufacturing Engineering Department, The Public Authority for Applied Education and Training, Shuweikh, Kuwait

Heat transfer enhancement in a horizontal annulus using the variable viscosity property of an Al_2O_3–water nanofluid is investigated. Two different viscosity models are used to evaluate heat transfer enhancement in the annulus. The base case uses the Pak and Cho model and the Brinkman model for viscosity which take into account the dependence of this property on temperature and nanoparticle volume fraction. The inner surface of the annulus is heated uniformly by a constant heat flux q_w and the outer boundary is kept at a constant temperature T_c. The nanofluid generates heat internally. The governing equations are solved numerically subject to appropriate boundary conditions by a penalty finite-element method. It is observed that for a fixed Prandtl number $Pr = 6.2$, Rayleigh number $Ra = 10^4$ and solid volume fraction $\phi = 10\%$, the average Nusselt number is enhanced by diminishing the heat generation parameter, mean diameter of nanoparticles, and diameter of the inner circle. The mean temperature for the fluids (nanofluid and base fluid) corresponding to the above mentioned parameters is plotted as well. © 2012 Wiley Periodicals, Inc. Heat Trans Asian Res, 41(6): 536–552, 2012; Published online 30 July 2012 in Wiley Online Library (wileyonlinelibrary.com/journal/htj). DOI 10.1002/htj.21016

Key words: annulus, natural convection, nanofluid, heat flux, heat transfer enhancement

1. Introduction

Natural convection heat transfer is an important phenomenon in engineering systems due to its wide applications in electronic cooling, heat exchangers, and thermal systems. Enhancement of heat transfer in such systems is very essential from industrial and energy saving perspectives. The low thermal conductivity of conventional heat transfer fluids, such as water, is considered a primary limitation in enhancing the performance and the compactness of such thermal systems. An innovative technique for the improvement of heat transfer using nano-scale particles dispersed in a base fluid, known as a nanofluid, has been studied extensively in recent years, according to Trisaksri and Wongwises [1] and Choi [2]. Daungthongsuk and Wongwises [3] examined it mainly in forced

convection applications. However, natural convection heat transfer research using nanofluids has received very little attention and there is still a debate on the effect of nanoparticles on heat transfer enhancement in natural convection applications. An example of these controversial results are the results reported by Khanafer et al. [4] who studied Cu–water nanofluids in a two-dimensional rectangular enclosure. They reported an increase in heat transfer with the increase in the percentage of suspended nanoparticles at any given Grashof number.

Oztop and Abu-Nada [5] showed similar results, where an enhancement in heat transfer was registered by the addition of nanoparticles. However, contrary experimental findings were reported by Putra et al. [6] using Al_2O_3 and CuO water nanofluids. They reported that the natural convection heat transfer coefficient was lower than that of a clear flow. Additionally, another experimental work in natural convection by Wen and Ding [7] reported deterioration in heat transfer caused by the addition of nanoparticles.

In fact, convective heat transfer is affected by the thermophysical properties of the nanofluid such as viscosity and thermal conductivity. A recent nanofluid heat transfer study on forced convection conducted by Mansour et al. [8] revealed that for forced convection different expressions for the thermophysical properties of nanofluids lead to totally different predictions for the performance of a system. Most recently, Abu-Nada et al. [9] showed that the enhancement of heat transfer in natural convection depended mainly on the Rayleigh number; and for certain Rayleigh numbers, $Ra = 10^4$, the heat transfer was not sensitive to nanoparticle concentration, whereas at higher values of Rayleigh number an enhancement in heat transfer was taking place. Therefore, there is still a controversy on the effect of nanofluids on heat transfer in natural convection and the numerical simulations seem to overestimate the enhancement of heat transfer in natural convection.

All of the previously mentioned numerical results conducted on natural convection used the Brinkman model for the viscosity. This model is shown to underestimate the effective viscosity of the nanofluid by Nguyen et al. [10] and Polidori et al. [11]. The Brinkman model does not consider the effect of nanofluid temperature or nanoparticle size. Besides, the Brinkman model was derived for larger particle size compared to the size of the nanoparticles. On the other hand, for thermal conductivity, most of the numerical simulations reported in literature used the Maxwell Garnett (MG) model [12]. This model does not consider the main mechanisms for heat transfer in nanofluids such as Brownian motion and does not consider nanoparticle size or temperature dependence.

Therefore, numerical simulations need more robust nanofluid models for viscosity and thermal conductivity that take into account temperature dependence and nanoparticle size. Angue Minsta et al. [13] studied the effect of nanoparticle concentration and nanoparticle size on nanofluid viscosity under a wide range of temperatures experimentally. They showed that the viscosity dropped sharply with temperature especially for a high concentration of nanoparticles. Moreover, the effects of temperature, nanoparticle size, and nanoparticle volume fraction on thermal conductivity were studied experimentally by Chon et al. [14]. They showed that the nanofluid thermal conductivity was also affected by temperature, volume fraction of nanoparticles, and nanoparticle size. Thus, such physics cannot be neglected and the dependence of nanofluid properties on temperature, and volume fraction of nanoparticles, must be taken into account in order to predict the correct role of nanoparticles on heat transfer enhancement. Lattice Boltzmann simulation of an alumina–water nanofluid in a square cavity was performed by He et al. [15], where they developed a lattice Boltzmann model by coupling

the density (D2Q9) and the temperature distribution functions with speed to simulate convection heat transfer utilizing Al_2O_3–water nanofluids in a square cavity.

Recently, Sankar and Younghae [16] performed numerically the simulation of free convection heat transfer in a vertical annular cavity with discrete heating. Their numerical results revealed that the heat transfer rate was always higher at the bottom heater. Also, the rate of heat transfer increased with the radii ratio but decreased with the aspect ratio. Further numerical simulation of free convection based on experimental measured conductivity in a square cavity using a water/SiO_2 nanofluid was conducted by Jahanshahi et al. [17] where an experimental setup had been used to extract the conductivity value of nanofluid. In the same year, Lotfi et al. [18] studied forced convective heat transfer of nanofluids with a comparison of different approaches. A two-phase Eulerian model was implemented for the first time to study such a flow field. The single-phase model and two-phase mixture model formulations were also used for comparison in their study.

Very recently, He et al. [19] investigated lattice Boltzmann simulation of an alumina–water nanofluid in a square cavity. The effects of Rayleigh number and nanoparticle volume fraction on natural convection heat transfer of a nanofluid were investigated in this study. Numerical results indicated that the flow and heat transfer characteristics of the Al_2O_3–water nanofluid in a square cavity were more sensitive to viscosity than to thermal conductivity. Sandipkumar et al. [20] conducted a study on the effect of particle size in aviation turbine fuel and Al_2O_3 nanofluids for heat transfer applications. They concluded that at 50 °C and 0.3% particle volume concentration, the bigger particles showed increases of 17% in thermal conductivity and 55% in viscosity, whereas the smaller particles showed corresponding increases of 21% and 22% for thermal conductivity and viscosity, respectively.

Nemati et al. [21] analyzed the mixed convection flow of three types of nanofluids in a lid-driven cavity using the same method. The results indicated that the effects of solid volume fraction grew stronger sequentially for Al_2O_3, CuO, and Cu. In addition the increases in Reynolds number lead to a decrease in the solid concentration effect. Shahi et al. [22] numerically performed a laminar conjugated-natural convection heat transfer enhancement of a nanofluid in an annular tube driven by an inner heat generating solid cylinder where the governing equations were derived based on the conceptual model in the cylindrical coordinate system and had been solved using the finite volume approach, using the SIMPLE algorithm on the collocated arrangement. Moghari et al. [23] conducted a two-phase mixed convection Al_2O_3–water nanofluid flow in an annulus. The calculated results showed that at a given *Re* and *Gr*, increasing the nanoparticle volume fraction increased the Nusselt number at the inner and outer walls while it did not have any significant effect on the friction factor. Both the Nusselt number and the friction coefficient at the inner wall were more than their corresponding values at the outer wall. This year, Fattahi et al. [24] studied a lattice Boltzmann simulation of natural convection heat transfer in nanofluids where the flow and heat transfer characteristics of the Al_2O_3–water nanofluid in the square cavity were more sensitive to viscosity than to thermal conductivity.

Therefore, the scope of the current research is to implement two different thermal conductivity models namely the Maxwell Garnett (MG) model used by Abu-Nada [25] and the Chon et al. [14] model for nanofluid properties and to study the effect of these models on heat transfer in natural convection. The flow field and enhancement in heat transfer are evaluated under wide ranges of the

internal heat generation parameter, the mean diameter of the nanoparticles, and the diameter of the inner circular surface.

Nomenclature

C_p: specific heat at constant pressure, kJ kg^{-1} K^{-1}
d: diameter of inner circle, m
D: non-dimensional diameter of inner circle, $D = d/(r_o - r_i)$
Dp: mean diameter of nanaoparticles, nm
g: gravitational acceleration, m s^{-2}
Gr: Grashof number, $Gr = g\beta(T_b - T_c)(r_o - r_i)^3/\nu_f^2$
h: local heat transfer coefficient, W m^{-2} K^{-1}
k: thermal conductivity, W m^{-1} K^{-1}
Nu: Nusselt number, $Nu = h(r_o - r_i)/k_f$
Pr: Prandtl number, $Pr = \nu_f/\alpha_f$
q: volumetric rate of heat generation, W/m^3
q_w: heat flux, W m^{-2}
Q: heat generation parameter, $Q = q(r_o - r_i)^2/\nu_f(T_h - T_i)$
r: dimensional radius of circle, m
R: dimensionless radius of circle
T: dimensional temperature, °K
u, v: dimensional x and y components of velocity, m s^{-1}
U, V: dimensionless velocities, $U = u/(r_o - r_i)$, $V = v/(r_o - r_i)$
X, Y: dimensionless coordinates, $X = x/(r_o - r_i)$, $Y = y/(r_o - r_i)$
x, y: dimensional coordinates, m

Greek Symbols

α: fluid thermal diffusivity, m^2 s^{-1}
β: thermal expansion coefficient, K^{-1}
ϕ: nanoparticle volume fraction
φ: angular coordinate, °
ν: kinematic viscosity, m^2 s^{-1}
θ: dimensionless temperature, $\theta = (T - T_c)/(T_b - T_c)$
ρ: density, kg m^{-3}
μ: dynamic viscosity, N s m^{-2}

Subscripts

b: boundary
c: cold
f: fluid
i: inner
nf: nanofluid
o: outer
s: solid particle

2. Problem Formulation

Figure 1 shows a schematic diagram of a differentially heated annulus. The fluid in the annulus is water-based nanofluid containing Al_2O_3 nanoparticles and generates heat internally. The nanofluid is assumed incompressible and the flow is considered to be laminar. It is taken that water and nanoparticles are in thermal equilibrium and no slip occurs between them. The inner circle with radius r_i is heated uniformly by a heat flux q and the outer circle of radius r_o is kept at a constant temperature T_c. The thermophysical properties of the nanofluid are given in Table 1. The density of the nanofluid is approximated by the Boussinesq model. The viscosity of the nanofluid is considered a variable property that varies with volume fraction of nanoparticles.

The governing equations for laminar, steady-state natural convection in an annulus filled with water–alumina nanofluid in terms of the Navier–Stokes and energy equations are given as

Continuity equation:

$$\frac{\partial u}{\partial x}+\frac{\partial v}{\partial y}=0 \tag{1}$$

x-momentum equation:

$$\rho_{nf}\left(u\frac{\partial u}{\partial x}+v\frac{\partial u}{\partial y}\right)=-\frac{\partial p}{\partial x}+\mu_{nf}\left(\frac{\partial^2 u}{\partial x^2}+\frac{\partial^2 u}{\partial y^2}\right) \tag{2}$$

y-momentum equation:

$$\rho_{nf}\left(u\frac{\partial v}{\partial x}+v\frac{\partial v}{\partial y}\right)=-\frac{\partial p}{\partial y}+\mu_{nf}\left(\frac{\partial^2 v}{\partial x^2}+\frac{\partial^2 v}{\partial y^2}\right)+g\rho_{nf}\beta_{nf}(T-T_c) \tag{3}$$

Energy equation:

$$u\frac{\partial T}{\partial x}+v\frac{\partial T}{\partial y}=\alpha_{nf}\left(\frac{\partial^2 T}{\partial x^2}+\frac{\partial^2 T}{\partial y^2}\right)+q \tag{4}$$

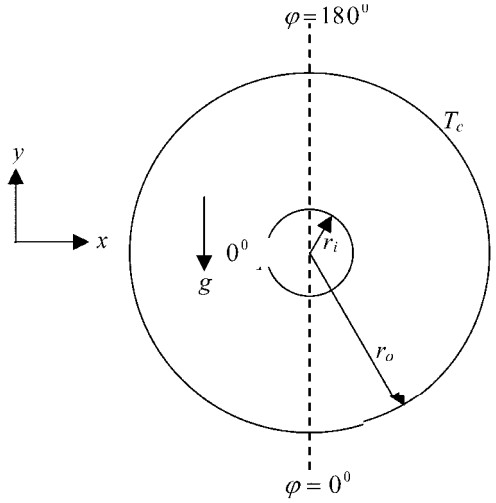

Fig. 1. Schematic diagram of the annulus and coordinate system.

Table 1. Thermophysical Properties of Fluid and Nanoparticles

Physical Properties	Fluid phase (Water)	Al_2O_3
C_p(J/kgK)	4179	765
ρ (kg/m^3)	997.1	3970
k (W/mK)	0.613	25
$\beta\times10^{-5}$ (1/K)	21	0.85

where $\rho_{nf} = (1-\phi)\rho_f + \phi\rho_s$ is the density, $(\rho C_p)_{nf} = (1-\phi)(\rho C_p)_f + \phi(\rho C_p)_s$ is the heat capacitance, $\beta_{nf} = (1-\phi)\beta_f + \phi\beta_s$ is the thermal expansion coefficient, and $\alpha_{nf} = k_{nf}/(\rho C_p)_{nf}$ is the thermal diffusivity.

The effective thermal conductivity of the nanofluid is approximated by the Chon et al. model [14]:

$$\frac{k_{nf}}{k_f} = 1 + 64.7\phi^{0.764}\left(\frac{d_f}{d_s}\right)^{0.369}\left(\frac{k_f}{k_s}\right)^{0.7476} Pr^{0.9955}\left(\frac{\rho_f k_b T}{3\pi\mu_f^2 l}\right)^{1.2321} \tag{5}$$

where k_b is the Boltzmann constant, 1.3807×10^{-23} J/K, and l is the mean path of the base fluid particles given as 0.17 nm (Chon et al. [14]).

This model is found to be appropriate for studying heat transfer enhancement using nanofluids by Abu-Nada [25]. In addition, the viscosity of the nanofluid can be approximated as viscosity of a base fluid μ_f containing a dilute suspension of fine spherical particles. In the current study, the viscosity of the nanofluid is considered by using two models, namely, the Pak and Cho correlation [26] and the Brinkman model [27]. These equations are given as

$$\mu_{nf} = \mu_f\left(1 + 39.11\phi + 533.9\phi^2\right) \text{ and} \tag{6}$$

$$\mu_{nf} = \mu_f\left(1-\phi\right)^{-2.5} \tag{7}$$

The above equations are non-dimensionalized by using the following dimensionless dependent and independent variables:

$$X = \frac{x}{\left(r_o - r_i\right)},\quad Y = \frac{y}{\left(r_o - r_i\right)},\quad U = \frac{u\left(r_o - r_i\right)}{\alpha_f},\quad V = \frac{v\left(r_o - r_i\right)}{\alpha_f},\quad D = \frac{d}{\left(r_o - r_i\right)}$$

$$P = \frac{p\left(r_o - r_i\right)^2}{\rho_f \alpha_f^{\,2}},\quad \theta = \frac{\left(T - T_c\right)k_f}{q_w\left(r_o - r_i\right)}$$

Then the corresponding dimensionless equations are

$$\frac{\partial U}{\partial X} + \frac{\partial V}{\partial Y} = 0 \tag{8}$$

$$U\frac{\partial U}{\partial X}+V\frac{\partial U}{\partial Y}=-\frac{\rho_f}{\rho_{nf}}\frac{\partial P}{\partial X}+Pr\frac{\nu_{nf}}{\nu_f}\left(\frac{\partial^2 U}{\partial X^2}+\frac{\partial^2 U}{\partial Y^2}\right) \tag{9}$$

$$U\frac{\partial V}{\partial X}+V\frac{\partial V}{\partial Y}=-\frac{\rho_f}{\rho_{nf}}\frac{\partial P}{\partial Y}+Pr\frac{\nu_{nf}}{\nu_f}\left(\frac{\partial^2 V}{\partial X^2}+\frac{\partial^2 V}{\partial Y^2}\right)+\ Ra\,Pr\frac{(1-\phi)\rho_f\beta_f+\phi\rho_s\beta_s}{\rho_{nf}\beta_f}\theta \tag{10}$$

$$U\frac{\partial \theta}{\partial X}+V\frac{\partial \theta}{\partial Y}=\frac{\alpha_{nf}}{\alpha_f}\left(\frac{\partial^2 \theta}{\partial X^2}+\frac{\partial^2 \theta}{\partial Y^2}\right)+Q \tag{11}$$

where $Pr = \nu_f/\alpha_f$ is the Prandtl number, $Ra = g\beta_f q_w(r_o - r_i)^4/\nu_f\alpha_f k_f$ is the Rayleigh number, and $Q = q(r_o - r_i)^2/\nu_f(T_h - T_c)$ is the internal heat generation parameter.

The corresponding boundary conditions take the following form:

at all solid boundaries $U = V = 0$

at the outer boundary $\theta = 0$

at the inner boundary $\partial\theta/\partial N = -1$

The local and average Nusselt numbers at the heated surface of the enclosure may be expressed, respectively, as

$$Nu_{local}=-\left(\frac{k_{nf}}{k_f}\right)\frac{\partial\theta}{\partial\varphi}\quad\text{and}\quad Nu=\frac{1}{2\pi}\int_0^{2\pi}Nu_{local}\,d\varphi \tag{12}$$

The mean temperature of the fluid in the enclosure is given by $\theta_{av} = \int\theta d\overline{V}/\overline{V}$, where $\overline{V}$ is the annulus volume.

3. Numerical Implementation

The Galerkin finite element method [28, 29] is used to solve the non-dimensional governing equations along with boundary conditions for the considered problem. The equation of continuity has been used as a constraint due to mass conservation and this restriction may be used to find the pressure distribution. The penalty finite element method [30] is used to solve Eqs. (9)–(11), where the pressure P is eliminated by a penalty constraint ξ, and the incompressibility criteria given by Eq. (8) which can be expressed as

$$P=-\xi\left(\frac{\partial U}{\partial X}+\frac{\partial V}{\partial Y}\right) \tag{13}$$

The continuity equation is automatically fulfilled for large values of ξ. Then the velocity components (U, V), and temperature (θ) are expanded using a basis set $\{\Phi\}_{k=1}^{N}$ as

$$U\approx\sum_{k=1}^{N}U_k\Phi_k(X,Y),\quad V\approx\sum_{k=1}^{N}V_k\Phi_k(X,Y)\ \text{and}\quad \theta\approx\sum_{k=1}^{N}\theta_k\Phi_k(X,Y) \tag{14}$$

The Galerkin finite element technique yields the subsequent nonlinear residual equations for Eqs. (9), (10), and (11) respectively at nodes of the internal domain Ω:

$$R_i^{(1)} = \sum_{k=1}^{N} U_k \int_\Omega \left[\left(\sum_{k=1}^{N} U_k \Phi_k \right) \frac{\partial \Phi_k}{\partial X} + \left(\sum_{k=1}^{N} V_k \Phi_k \right) \frac{\partial \Phi_k}{\partial Y} \right] \Phi_i dXdY -$$
$$\xi \frac{\rho_f}{\rho_{nf}} \left[\sum_{k=1}^{N} U_k \int_\Omega \frac{\partial \Phi_i}{\partial X} \frac{\partial \Phi_k}{\partial X} dXdY + \sum_{k=1}^{N} V_k \int_\Omega \frac{\partial \Phi_i}{\partial Y} \frac{\partial \Phi_k}{\partial Y} dXdY \right] -$$
$$Pr \frac{\nu_{nf}}{\nu_f} \sum_{k=1}^{N} U_k \int_\Omega \left[\frac{\partial \Phi_i}{\partial X} \frac{\partial \Phi_k}{\partial X} + \frac{\partial \Phi_i}{\partial Y} \frac{\partial \Phi_k}{\partial Y} \right] dXdY \tag{15}$$

$$R_i^{(2)} = \sum_{k=1}^{N} V_k \int_\Omega \left[\left(\sum_{k=1}^{N} U_k \Phi_k \right) \frac{\partial \Phi_k}{\partial X} + \left(\sum_{k=1}^{N} V_k \Phi_k \right) \frac{\partial \Phi_k}{\partial Y} \right] \Phi_i dXdY -$$
$$\xi \frac{\rho_f}{\rho_{nf}} \left[\sum_{k=1}^{N} U_k \int_\Omega \frac{\partial \Phi_i}{\partial X} \frac{\partial \Phi_k}{\partial X} dXdY + \sum_{k=1}^{N} V_k \int_\Omega \frac{\partial \Phi_i}{\partial Y} \frac{\partial \Phi_k}{\partial Y} dXdY \right] - Pr \frac{\nu_{nf}}{\nu_f}$$
$$\sum_{k=1}^{N} V_k \int_\Omega \left[\frac{\partial \Phi_i}{\partial X} \frac{\partial \Phi_k}{\partial X} + \frac{\partial \Phi_i}{\partial Y} \frac{\partial \Phi_k}{\partial Y} \right] dXdY - Ra\, Pr \frac{(1-\phi)\rho_f \beta_f + \phi \rho_s \beta_s}{\rho_{nf} \beta_f} \int_\Omega \left(\sum_{k=1}^{N} \theta_k \Phi_k \right) \Phi_i dXdY \tag{16}$$

$$R_i^{(3)} = \sum_{k=1}^{N} \theta_k \int_\Omega \left[\left(\sum_{k=1}^{N} U_k \Phi_k \right) \frac{\partial \Phi_k}{\partial X} + \left(\sum_{k=1}^{N} V_k \Phi_k \right) \frac{\partial \Phi_k}{\partial Y} \right] \Phi_i dXdY -$$
$$\frac{\alpha_{nf}}{\alpha_f} \sum_{k=1}^{N} \theta_k \int_\Omega \left[\frac{\partial \Phi_i}{\partial X} \frac{\partial \Phi_k}{\partial X} + \frac{\partial \Phi_i}{\partial Y} \frac{\partial \Phi_k}{\partial Y} \right] dXdY - Q \tag{17}$$

Three-point Gaussian quadrature is used to evaluate the integrals in these equations. The non-linear residual Eqs. (15), (16), and (17) are solved using the Newton–Raphson method to determine the coefficients of the expansions in Eq. (14). The convergence of solutions is assumed when the relative error for each variable between consecutive iterations is recorded below the convergence criterion ε such that $|\Psi^{n+1} - \Psi^n| \le 10^{-4}$, where n is the number of iterations and Ψ is a function of U, V, and θ.

4. Mesh Generation

In the finite element method, mesh generation is the technique to subdivide a domain into a set of sub-domains, called finite elements, control volume, etc. The discrete locations are defined by the numerical grid, at which the variables are to be calculated. It is basically a discrete representation of the geometric domain on which the problem is to be solved. The computational domains with irregular geometries by a collection of finite elements make the method a valuable practical tool for the solution of boundary value problems arising in various fields of engineering. Figure 2 displays the finite element mesh of the present physical domain.

4.1 Grid-independent test

An extensive mesh testing procedure is conducted to guarantee a grid-independent solution for $Ra = 10^4$, $Pr = 6.2$, $\phi = 10\%$, $Q = 0$, $Dp = 5$, and $D = 0.2$ in a horizontal annulus. In the present work, we examine five different non-uniform grid systems with the following number of elements

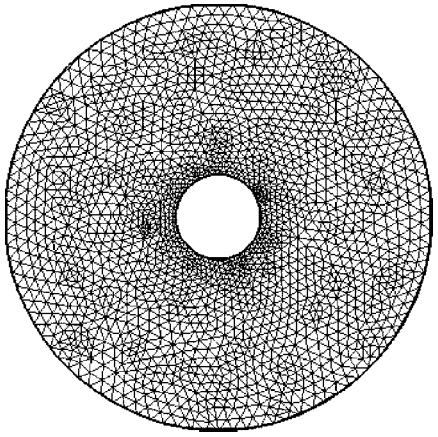

Fig. 2. Mesh generation of the annulus.

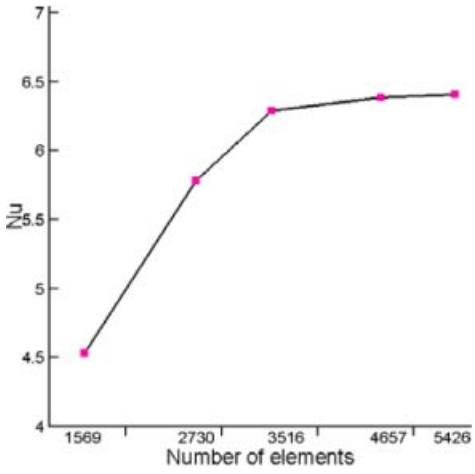

Fig. 3. Grid-independency study for $Pr = 6.2$, $Gr = 10^4$, $Q = 1$, $Dp = 5$, $D = 0.2$, and $\phi = 10\%$. [Color figure can be viewed in the online issue, which is available at wileyonlinelibrary.com/journal/htj.]

within the resolution field: 1569, 2730, 3516, 4657, and 5426. The numerical scheme is carried out for a highly precise key in the average Nusselt number *Nu* for the aforesaid elements to develop an understanding of the grid fineness as shown in Fig. 3. The corresponding detail data is displayed in Table 2. The scale of the average Nusselt number for 4657 elements shows little difference with the results obtained for the other elements. Hence, considering the non-uniform grid system of 4657 elements is preferred for the computation.

4.2 Code validation

The model validation is an important part of a numerical investigation. Hence, the outcome of the present numerical code is benchmarked against the numerical result of Abu-Nada [16] which was reported for the effects of variable viscosity and thermal conductivity of Al_2O_3–water nanofluid on heat transfer enhancement in natural convection in an annulus. The comparison is conducted while employing the dimensionless parameters $Ra = 10^5$, $L/D = 0.8$, $\phi = 4\%$, and $Pr = 0.7$ for both the streamlines and isotherms. This validation boosts the confidence in our numerical code to carry on

Table 2. Grid Sensitivity Check at $Pr = 6.2$, $Gr = 10^4$, $Q = 1$, $Dp = 5$, $D = 0.2$, and $\phi = 10\%$

Nodes (elements)	2224 (1569)	5148 (2730)	9538 (3516)	13295 (4657)	18524 (5426)
Nu	4.52945	5.78176	6.28701	6.38701	6.40701
Time (s)	226.265	292.594	388.157	421.328	627.375

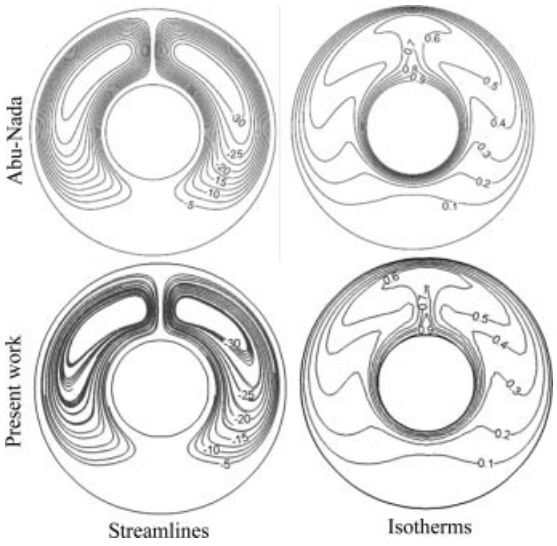

Fig. 4. Comparison between present work and Abu-Nada [21] for $Ra = 10^5$, $L/D = 0.8$, $\phi = 4\%$, and $Pr = 0.7$.

with the above-stated objective of the current investigation. As shown in Fig. 4, the new model is able to reproduce the published result of Abu-Nada [25].

5. Results and Discussion

In this section, numerical results of streamlines and isotherms for various values of the heat generation parameter Q, mean diameter of the nanoparticles Dp, and the diameter of inner cirle D are displayed. The considered values of Q, Dp, and D are Q (= 0, 1, 5, and 10), Dp (= 5, 25, 50, and 100) and D (= 0.1, 0.2, 0.4, and 0.6). For this investigation, Rayleigh number (Ra), Prandtl number (Pr), and solid volume fraction (ϕ) are kept fixed at 10^4, 6.2, and 10%, respectively. In addition, the values of the local and average Nusselt numbers as well as mean temperature of the nanofluid in the annulus have been calculated for different mentioned parameters for both the Pak and Cho correlation [26] and the Brinkman model [27].

Figures 5(a) and 5(b) indicate the influence of different values of the internal heat generation parameter (Q) on the velocity and temperature profiles in an annulus filled with water–alumina nanofluid while Dp and D are fixed at 5 and 0.2, respectively. The streamlines and isotherms for both models are almost similar. For $Q = 0$, the flow field is characterized by two primary revolving cells that occupy the bulk of the annulus. The right and left eddies move in clockwise and counter-clockwise directions, respectively. In addition it appears from Fig. 5(a) that the overall feature of the streamlines is not perturbed by varying Q from 0 to 10 in the free convection regime except when the size of the cells reduces.

The corresponding isothermal lines in Fig. 5(b) become more bent and take a circular shape in the upper and lower portions of the annulus, respectively, whereas initially ($Q = 0$), they are almost flat. It is important to note that the isotherms are clustered near the heat source of the annulus for the

absence of internal heat generation. This indicates a temperature gradient in the normal direction in this region. The strength of the flow circulation is much higher for high Q values. The thick boundary layer diminishes with the escalating values of Q. In addition, the isothermal lines occupy the whole annulus due to the fact that an increase in Q raises the internal energy of the fluid. This is true for both models. However, the increase in the thermal gradients at the heated inner circular surface is much higher for the Pak and Cho model [26] than for the Brinkman model [27]. This means that higher heat transfer rates are predicted by the Pak and Cho model [26] than for the Brinkman model [27] as will be seen in the subsequent figures.

To study the effect of the mean nanoparticle diameter on the heat transfer, the nanoparticle diameter is varied between 5 nm and 100 nm, while $Q = 1$ and $D = 0.2$. The streamlines and temperature contours are presented in Figs. 6(a) and 6(b). As the mean nanoparticle diameter increases, the corresponding velocity boundary layer grows down and hence the heat transfer enhancement is reduced. Notice that the fluids suspended with Al_2O_3 nanoparticles for the Pak and Cho model [26]

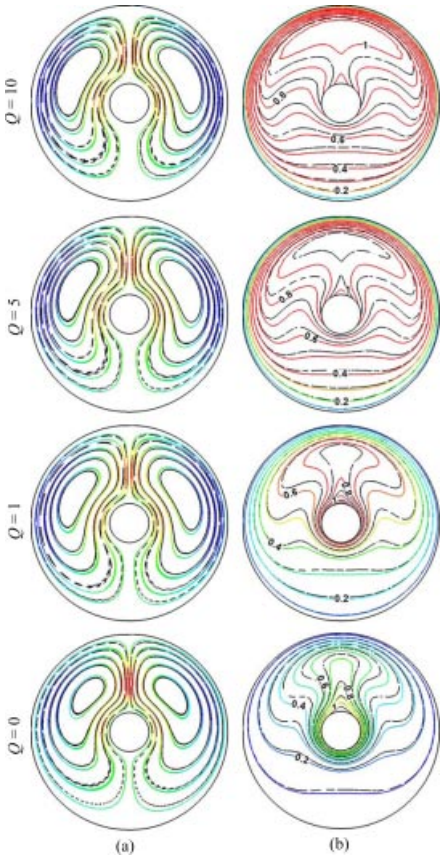

Fig. 5. Effect of Q on (a) streamlines and (b) isotherms with $Dp = 5$, $D = 0.2$ (colored lines for Pak and Cho model and black lines for Brinkman model). [Color figure can be viewed in the online issue, which is available at wileyonlinelibrary.com/journal/htj.]

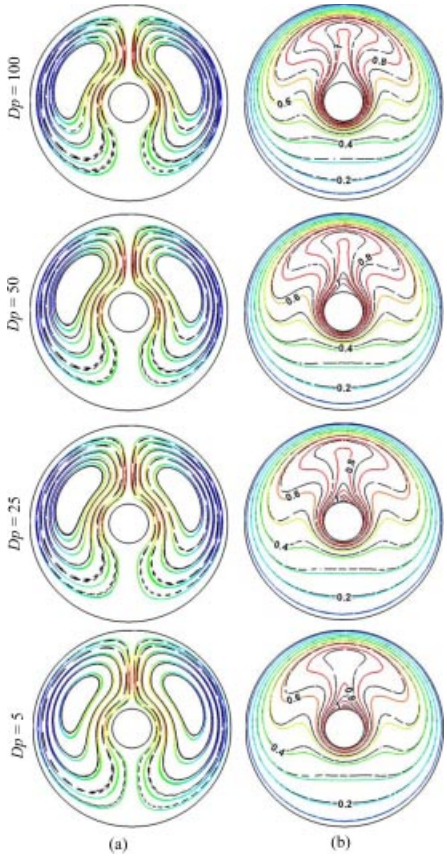

Fig. 6. Effect of Dp on (a) streamlines and (b) isotherms with $Q = 1$, $D = 0.2$ (colored lines for Pak and Cho model and black lines for Brinkman model). [Color figure can be viewed in the online issue, which is available at wileyonlinelibrary.com/journal/htj.]

mitigate the fluid flow in the annulus, except for $Dp = 5$ nm, when compared with the Brinkman model [27]. This phenomenon is mainly caused by the effective dynamic viscosity, which dominates the heat transfer characteristic of the nanofluid flow. Two circular cells are formed at relatively low values of the mean diameter of the nanoparticles (Dp). The shape of these cells becomes smaller with a growing Dp. The value of the absolute circulation strength and the thermal current activities lessen with an increase in the mean nanoparticle diameter for both models. It is worth noting that as the mean diameter of the nanoparticles decreases, the thickness of the thermal plume above the inner cylinder increases which indicates a steep temperature gradient and hence an increase in the overall heat transfer within the annulus. This fact, due to a solid concentration of nanoparticles, does not have considerable effect when the buoyancy force is low at the conduction mode.

The effect of the physical parameter (diameter of inner circle D) on the velocity and temperature profiles is depicted in Figs. 7(a) and 7(b) when $Q = 1$ and $Dp = 5$. It is important to note that with the variation of D from 0.1 to 0.6, a similarity in the velocity and temperature fields between the two types of considered models is observed. The vortices created in the velocity field become compressed near the outer surface due to the enhanced physical parameter. The corresponding isothermal lines are also clustered. The strength of the flow circulation and the thermal current

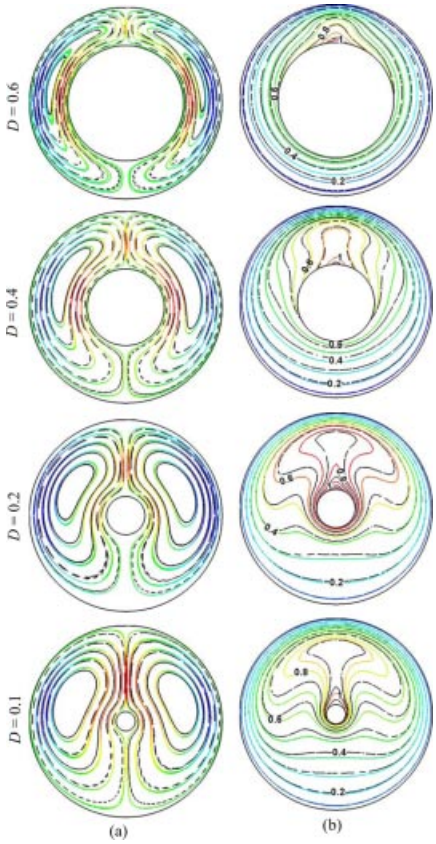

Fig. 7. Effect of D on (a) streamlines and (b) isotherms with $Q = 1$, $Dp = 5$ (colored lines for Pak and Cho model and black lines for Brinkman model). [Color figure can be viewed in the online issue, which is available at wileyonlinelibrary.com/journal/htj.]

activities are much more activated with the falling D. For $D = 0.6$, the isothermal lines become more circular than the case of $D = 0.1$ in the entire region of the annulus. This is true for both the considered models. However, the increase in the thermal gradients is much higher for the Pak and Cho model [26] than for the Brinkman model [27]. This means that higher heat transfer rates are predicted by the Pak and Cho model [26] than for the Brinkman model [27] for diminishing values of D as seen in Fig. 7(b).

The average Nusselt number (Nu) along the hot surface from the numerical results for various values of Q, Dp, and D are depicted in Figs. 8(i)–8(iii), respectively. It is well known that Nu, a

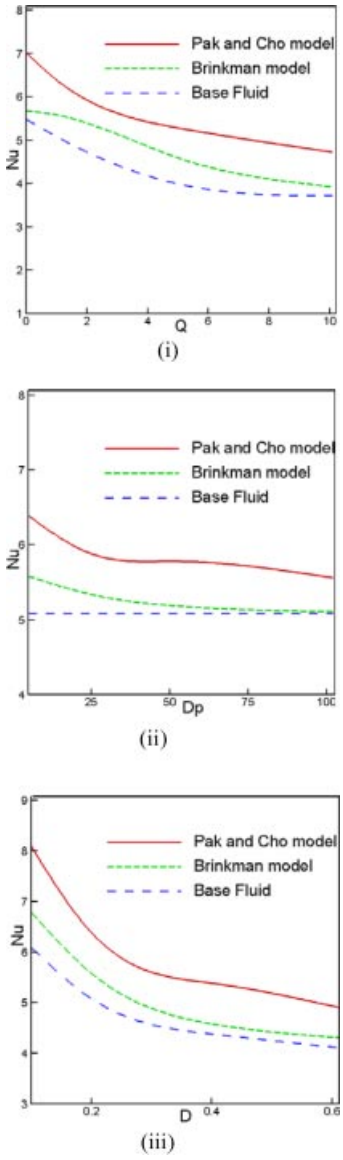

Fig. 8. Plots of (i) Nu with Q, (ii) Nu with Dp, and (iii) Nu with D. [Color figure can be viewed in the online issue, which is available at wileyonlinelibrary.com/journal/htj.]

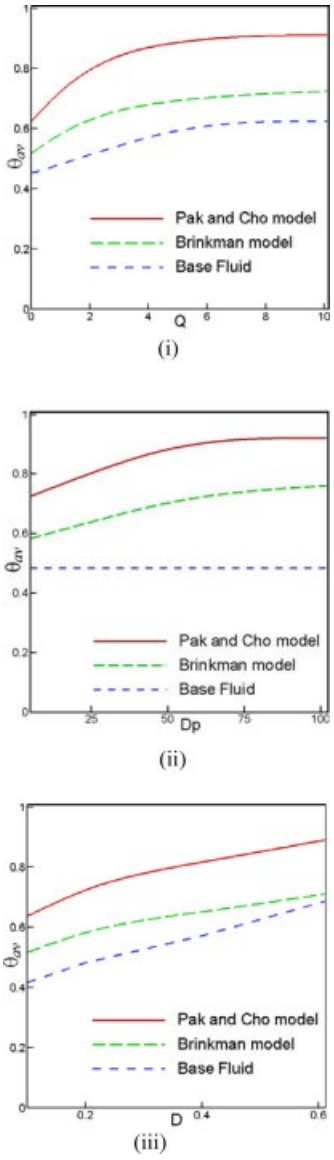

Fig. 9. Average temperature of the fluid inside the annulus for the influences of (i) *Q*, (ii) *Dp*, and (iii) *D*. [Color figure can be viewed in the online issue, which is available at wileyonlinelibrary.com/journal/htj.]

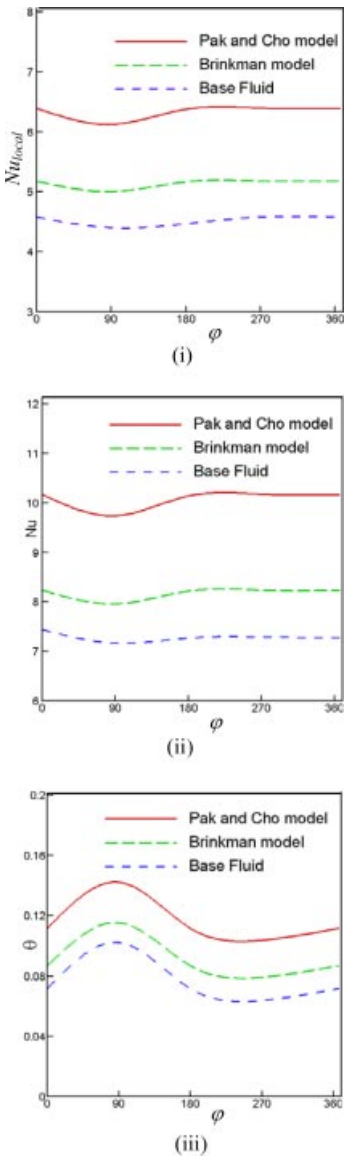

Fig. 10. Plots of (i) Nu_{local}, (ii) *Nu*, and (iii) temperature distribution with angular displacement φ. [Color figure can be viewed in the online issue, which is available at wileyonlinelibrary.com/journal/htj.]

measure of heat transfer, is optimized at the lowest *Q*, *Dp*, and *D* for the Pak and Cho model [26], the Brinkman model [27], and clear water. In the case of a nanofluid, the heat transfer rate is more effective for the Pak and Cho model [26] than for the Brinkman model [27]. But when compared to the base fluid, this rate of heat transfer is more effective for a nanofluid as shown in Figs. 8(ii)–8(iii). This mitigation of heat transfer is mainly attributed to the effective dynamic viscosity which is predominant in the natural convection of nanofluids for low effective thermal conductivity.

As $Q = q(r_o - r_i)^2/\nu_f(T_h - T_c)$, so increasing heat generation decreases the temperature difference between hot and cold boundaries. Thus the rate of heat transfer diminishes. Again a rising D enhances the heated portion of the annulus. So the average heat transfer decreases. As the mean nanoparticle diameter Dp increases, the corresponding flow velocity decreases and hence the heat transfer enhancement is reduced. Notice that the fluids suspended with Al_2O_3 nanoparticles mitigate the fluid flow in the cavity except for $Dp = 5$ nm when compared with the pure fluid. This phenomenon is mainly caused by the effective dynamic viscosity, which dominates the heat transfer characteristic of the nanofluid flow as the k_{nf}/k_f reaches unity.

Furthermore, the percent devalues in Nu for the increases in the parameters Q and D using the Pak and Cho model [26], Brinkman model [27], and the base fluid ($\phi = 0\%$) are 32%, 30%, and 26%, respectively, and 39%, 36%, and 32%, respectively. The average Nusselt number increases by 12% and 8% as the mean nanoparticle diameter is reduced from 100 to 5 nm with the Pak and Cho model [26] and Brinkman model [27], respectively.

Figures 9(i)–9(iii) plot the mean temperature (θ_{av}) for both type of fluids in the annulus for the controlling parameters Q, Dp, and D. It is observed from these figures that θ_{av} grows sequentially with increasing values of Q, Dp, and D. This is expected because growing values of these parameters enhance the potency of thermal behavior inside the boundary layer.

The local Nusselt number (Nu_{local}), average Nusselt number (Nu), and the bulk temperature (θ) along with the angular displacement φ are depicted in Figs. 10(i)–10(iii). The values of Nu_{local} and Nu diminish slightly up to $\varphi = 90°$ and beyond this region they rise for the case of a nanofluid ($\phi = 10\%$) using both employed models and base fluid ($\phi = 0\%$). Also, the bulk temperature of the fluid (nano and pure) grows sharply up to $\varphi \leq 90°$ and in the region $90° < \varphi \leq 360°$ it grows down sequentially. Using the Pak and Cho model [26], the temperature distribution is higher than the Brinkman model [27] as well as the clear water case.

6. Conclusion

The current investigation is concerned with heat and fluid flow of natural convection in an annulus with a water–alumina nanofluid. The results of this work illustrate that the heat transfer characteristics of the nanofluid can be enhanced as the nanoparticle mean diameter is reduced from 100 nm to 5 nm. These phenomena can be attributed to the dominant effect of the Brownian motion caused by heat convection. The increase of nanofluid temperature is found to augment the mean nanoparticle diameter inside the annulus. However, the heat transfer rate of the nanofluid compared with the pure fluid becomes more significant as the dimensionless internal heat generation parameter and the diameter of inner circle reduce from 10 to 0 and 0.6 to 0.1, respectively. This effect of nanofluids is mainly caused by the effective dynamic viscosity. The mean temperature (θ_{av}) of the fluids inside the boundary layer is also established for the effect of Q, Dp, and D where transport activities can be manipulated. For variable viscosity considering this geometry, the Pak and Cho model [26] plays a more momentous role for transferring heat than the Brinkman model [27]. Future work is recommended to extend the current investigation to a model with concentration distributions of nanoparticles. This model will aid in examining the contribution of the effect of particle migration in augmenting the heat transfer in the present configuration.

Literature Cited

1. Trisaksri V, Wongwises S. Critical review of heat transfer characteristics of nanofluids. Renewable Sustainable Energy Reviews 2007;11:512–523.
2. Choi US. Enhancing thermal conductivity of fluids with nanoparticles. In: Siginer, D.A., Wang, H.P. (Eds.), Developments and applications of non-Newtonian flows. ASME, New York, FED – 1995;231/MD–66:99–105.
3. Daungthongsuk W, Wongwises S. A critical review of convective heat transfer nanofluids. Renewable Sustainable Energy Reviews 2007;11:797–817.
4. Khanafer K, Vafai K, Lightstone M. Buoyancy-driven heat transfer enhancement in a two-dimensional enclosure utilizing nanofluids. Int J Heat Mass Transf 2003;46:3639–3653.
5. Oztop HF, Abu-Nada E. Numerical study of natural convection in partially heated rectangular enclosure filled with nanofluids. Int J Heat Fluid Flow 2008;29:1326–1336.
6. Putra N, Roetzel W, Das SK. Natural convection of nano-fluids. Heat Mass Transf 2003;39:775–784.
7. Wen D, Ding Y. Natural convective heat transfer of suspensions of titanium dioxide nanoparticles (nanofluids). IEEE Trans Nanotechnol 2006;5(3):220–227.
8. Mansour RB, Galanis N, Nguyen CT. Effect of uncertainties in physical properties on forced convection heat transfer with nanofluids. Appl Therm Eng 2007;27(1):240–249.
9. Abu-Nada E, Masoud Z, Hijazi A. Natural convection heat transfer enhancement in horizontal concentric annuli using nanofluids. Int Commun Heat Mass Transf 2008;35(5):657–665.
10. Nguyen CT, Desgranges F, Roy G, Galanis N, Mare T, Boucher S, Angue Minsta H. Temperature and particle-size dependent viscosity data for waterbased nanofluids–hystresis phenomenon. Int J Heat Fluid Flow 2007;28:1492–1506.
11. Polidori G, Fohanno S, Nguyen CT. A note on heat transfer modeling of Newtonian nanofluids in laminar free convection. Int J Therm Sci 2007;46(8):739–744.
12. Maxwell-Garnett JC. Colours in metal glasses and in metallic films. Philos Trans Roy Soc A 1904;203:385–420.
13. Angue Minsta H, Roy G, Nguyen CT, Doucet D. New temperature and conductivity data for water-based nanofluids. Int J Therm Sci 2009;48:363–371.
14. Chon CH, Kihm KD, Lee SP, Choi SUS. Empirical correlation finding the role of temperature and particle size for nanofluid (Al_2O_3) thermal conductivity enhancement. Appl Phys Lett 2005;87(97):153107.
15. Yurong He, Cong Qi, Yanwei Hu, Bin Qin, Fengchen Li, Yulong Ding. Lattice Boltzmann simulation of alumina-water nanofluid in a square cavity. Nanoscale Research Letters 2011;6(1):184–191.
16. Sankar M, Younghae Do. Numerical simulation of free convection heat transfer in a vertical annular cavity with discrete heating. Int Commun Heat Mass Transf 2010;37(6)600–606.
17. Jahanshahi M, Hosseinizadeh SF, Alipanah M, Dehghani A, Vakilinejad GR. Numerical simulation of free convection based on experimental measured conductivity in a square cavity using Water/SiO_2 nanofluid. Int Commun Heat Mass Transf 2010;37(6):687–694.
18. Lotfi R, Saboohi Y, Rashidi AM. Numerical study of forced convective heat transfer of nanofluids: Comparison of different approaches. Int Commun Heat Mass Transf 2010;37(1):74–78.
19. Yurong He, Cong Qi, Yanwei Hu, Bin Qin, Fengchen Li, Yulong Ding. Lattice Boltzmann simulation of alumina-water nanofluid in a square cavity. Nanoscale Res Lett 2011;6:184.
20. Sandipkumar Sonawane, Upendra Bhandarkar, Bhalchandra Puranik, S. Sunil Kumar. Effect of particle size in aviation turbine fuel-Al_2O_3 nanofluids for heat transfer applications. World Academy of Science, Engineering and Technology 2011;81.

21. Nemati H, Farhadi M, Sedighi K, Fattahi E, Darzi AAR. Lattice Boltzmann simulation of nanofluid in lid-driven cavity. Int Commun Heat Mass Transf 2010;37(10):1528–1534.
22. Shahi M, Mahmoudi AH, Talebi F. A numerical investigation of conjugated-natural convection heat transfer enhancement of a nanofluid in an annular tube driven by inner heat generating solid cylinder. Int Commun Heat Mass Transf 2011;38(4):533–542.
23. Moghari RM, Akbarinia A, Shariat M, Talebi F, Laur R. Two phase mixed convection Al_2O_3–water nanofluid flow in an annulus. Int J Multiphase Flow 2011;37(6):585–595.
24. Fattahi E, Farhadi M, Sedighi K, Nemati H. Lattice Boltzmann simulation of natural convection heat transfer in nanofluids. Int J Therm Sci 2012;52:137–144.
25. Abu-Nada E. Effects of variable viscosity and thermal conductivity of Al_2O_3–water nanofluid on heat transfer enhancement in natural convection. Int J Heat Fluid Flow 2009;30:679–690.
26. Pak BC, Cho Y. Hydrodynamic and heat transfer study of dispersed fluids with submicron metallic oxide particle. Exp Heat Transf 1998;11:151–170.
27. Brinkman HC. The viscosity of concentrated suspensions and solution. J Chem Phys 1952;20:571–581.
28. Taylor C, Hood P. A numerical solution of the Navier-Stokes equations using finite element technique, 1. Comput Fluids 1973;1:73–89.
29. Dechaumphai P. Finite element method in engineering, 2nd ed. Chulalongkorn University Press; 1999.
30. Basak T, Roy S, Pop I. Heat flow analysis for natural convection within trapezoidal enclosures based on heatline concept. Int J Heat Mass Transf 2009;52:2471–2483.

□♦ ♦ ♦□